Application of mean-field and surface-hopping approaches for interrogation of the Xe_3^+ molecular ion photoexcitation dynamics

Steven L. Fiedler,[1] Henrik M. Kunttu,[2] and J. Eloranta[3,a)]
[1]*Department of Mechanical Engineering, 2250 G.G. Brown, 2350 Hayward St., The University of Michigan, Ann Arbor, Michigan 48109-2125, USA*
[2]*Nanoscience Center, Department of Chemistry, P.O. Box 35, University of Jyväskylä, Jyväskylä 40014, Finland*
[3]*Department of Chemistry and Biochemistry, California State University at Northridge, 18111 Nordhoff St., Northridge, California 91330-8262, USA*

(Received 7 February 2008; accepted 26 March 2008; published online 28 April 2008)

The dissociation dynamics of the excited Xe_3^+ molecular ion through the $\Pi(1/2)_u$ and $\Pi(1/2)_g$ conical intersection was interrogated by computational simulation in which no adjustable parameters were used. The electronic ground and excited state potential energy surfaces were generated by the diatomics-in-molecules method, and the Ehrenfest mean-field and Tully surface-hopping approaches treated the nonadiabatic interactions. Reproduction of the experimental spectrum of the symmetric photofragmentation as a function of excitation energy was obtained within the region of interest (2.5–3.75 eV), with the exception of a 0.25 eV width on the red side of the spectral apex. Good agreement was obtained with the experimental dissociated photofragment kinetic energy spectra. It was determined that the greatest contribution to the nonadiabatic coupling between the two states originated from the bending vibrational mode of the molecule in the $\Sigma(1/2)_u$, ground electronic state before excitation. © *2008 American Institute of Physics*.
[DOI: 10.1063/1.2911697]

I. INTRODUCTION

Simulation of molecular dynamics (MD) of systems that cross, or nearly cross potential energy surfaces, requires considerations of the coupling between electronic and nuclear motions. The Born–Oppenheimer approximation is consequently inadequate, and thus such systems present an opportunity to view normally subtle time dependent quantum effects. From a computational perspective, nonadiabatic dynamics simulations that include consideration of the presence of multiple electronic states are significantly more expensive than adiabatic dynamics where atomic trajectories follow a single adiabatic potential energy hypersurface. To economize, semiclassical approaches have been developed which employ quantum mechanics based methods to calculate the electronic structure and coupling to the nuclei, while propagating the nuclei according to classical equations of motion.[1,2] Although many semiclassical approaches have been developed,[3] the Erhenfest or mean-field[4] and surface-hopping[5] approaches are often used[6–8] because of their relative simplicity and proven ability to quantitatively reproduce experimental spectra from photoexcitation and scattering measurements.[9–11]

Electronic structure calculations themselves can also require significant computational resources. Dynamics employing all electron *ab initio* calculations are currently restricted to few atoms with a limited number of electrons. For larger polyatomic systems, atomistic forces are calculated on the fly to eliminate the necessity to pretabulate potentials as required in grid-based methods. Semiempirical electronic structure methods can also provide an additional reduction in computational costs. One such approach, the valence-bond based diatomics-in-molecules (DIM) method,[12] has found particular favor as it is capable of calculating energetics to spectroscopic accuracy, while its computational speed allows for its inclusion in nonadiabatic calculations. For molecules containing heavy atoms, it has been shown[13,14] that DIM can incorporate spin-orbit coupling. A difficulty created upon the introduction of spin-orbit coupling into nonadiabatic dynamical formalism though resides in the fact that the eigenfunctions cannot be uniquely defined in complex space. This problem is reflected in the calculation of the nonadiabatic coupling vector, a fundamental quantity required by both the mean-field and surface-hopping approaches, which is dependent on the eigenfunctions. A few studies have addressed this problem, and various procedures have been proposed to accurately account for the eigenvector phase evolution.[8,15–17]

The focus of this study was to explore the conical intersection between the $\Pi(1/2)_g$ and $\Pi(1/2)_u$ states of the Xe_3^+ molecular ion, as shown in the circled region, Fig. 1(c). In particular, this triatomic system was well suited for implementation and testing of the applicability and limitations of the simulation methods described above. The two states were energetically well separated from other states and only couple with one other state, $\Sigma(1/2)_u$ in dissociated limit. This contrasts with the study of the Ar_3^+ system[18,19] where the dense manifold of states could require a more complex analysis. The limited number of atoms allowed efficient use of computational resources, and the conical intersection was

a)Author to whom correspondence should be addressed. Electronic mail: jussi.eloranta@csun.edu. Tel.: (818) 677-2677. FAX: (818) 677-4068.

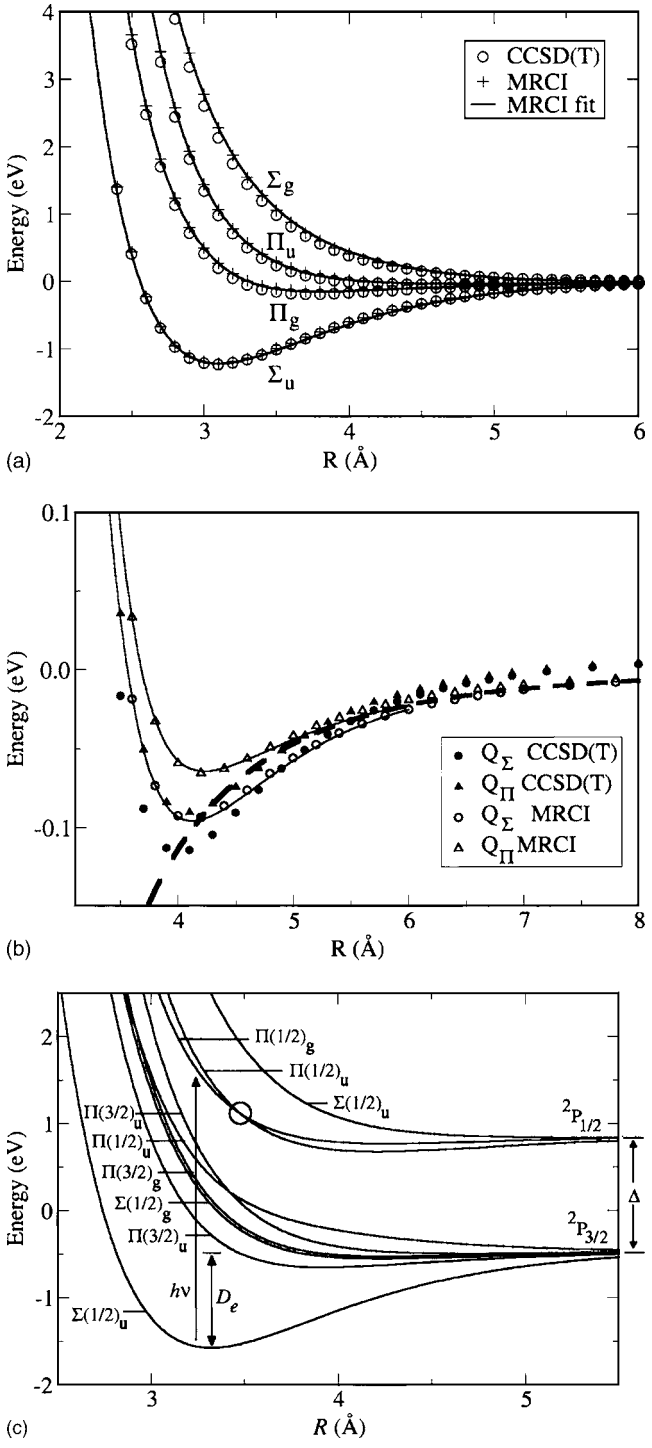

FIG. 1. (a) Xe_2^+ valence potential energy values as calculated by CCSD(T) (○) and MRCI (+) methods. Potential fits, based on Eqs. (6) and (7), are displayed as solid lines. (b) Xe_2^+ Coulombic potentials $Q(r)$, where $Q(r) = \frac{1}{2}(V_u(r) + V_g(r))$. Σ and Π potentials are displayed as circles and triangles, respectively, with values calculated by the CCSD(T) (solid symbols) and MRCI (hollow symbols). The ion-induced dipole contribution $-\alpha e^2/2r^4$ is shown for comparison (dashed line). Discussion contained in text. (c) Xe_3^+ symmetric stretch potential energy surfaces as a function of nearest neighbor separation R calculated in this study by the DIM method. The states are labeled according to their term symbols of their irreducible representations in the $D_{\infty h}$ point group. Also shown are the ground state binding energy D_e and the $^2P_{1/2}$ and $^2P_{3/2}$ Xe^+ fragment states separated in energy by the value of the spin-orbit splitting Δ.

energetically accessible for exploration by measurement: Haberland *et al.*[19] coupled optical excitation of rare gas trimeric ions including Xe_3^+ with an analysis of time-of-flight velocities of neutral and ionic photofragments. Differences in the highest occupied molecular orbital structure of the repulsive $\Pi(1/2)_g$ and $\Pi(1/2)_u$ states relegated the initial charge localized to different locations, specifically the outer and center atom(s), respectively. Upon subsequent dissociation, the ratio of "fast" versus "slow" particles could delineate the final population in each state. To gain further insight and dissect the contribution from each of the four vibrational modes to the above analysis, a study such as the one undertaken in this report was required, which employed the computational tools discussed above.

II. METHOD

A. Potential energy surfaces: Formalism and parametrization

As employed in previous studies,[13,20] the Hamiltonian matrix construct was based on the DIM method. Since DIM is based on the valence-bond method, molecular electronic state wavefunctions are expressed as a product of its constituent atomic-state wavefunctions. The basis states for the three dimensional wavefunction of Xe_3^+ form a vector,

$$\Psi = [p_{x,0}^{\alpha}\ p_{y,0}^{\alpha}\ p_{z,0}^{\alpha}\ p_{x,1}^{\alpha}\ \cdots\ p_{z,2}^{\beta}], \tag{1}$$

where α and β denote spin angular momenta for cation "hole" localized on Xe atoms labeled 0, 1, and 2.[21] The corresponding 18×18 dimensional Hamiltonian matrix was constructed, following the atoms-in-molecules approach,[22] as a sum of electronic and spin-orbit terms,

$$\mathbf{H} = \mathbf{H}_{\mathrm{el}} + \mathbf{H}_{\mathrm{S.O.}} = \mathbf{H}_{\mathrm{el.}} + \Delta\mathbf{l}\cdot\mathbf{s}, \tag{2}$$

where Δ, the Xe^+ spin-orbit splitting (1.31 eV),[23,24] was taken to be independent of nuclear configuration.

The electronic Hamiltonian $\mathbf{H}_{\mathrm{el}}$ was comprised as a sum of diatomic Hamiltonians $\mathbf{H}_{ij}$ with the positive charge delocalized between atoms i and j. Rotational matrices $\mathbf{R}_{ij}$ were used to rotate the diatomic Hamiltonians from their respective molecular frames to a common laboratory frame. In this manner, $\mathbf{H}_{\mathrm{el}}$ can be expressed as

$$\mathbf{H}_{\mathrm{el}} = \mathbf{R}_{01}^{-1}\mathbf{H}_{01}\mathbf{R}_{01} + \mathbf{R}_{02}^{-1}\mathbf{H}_{02}\mathbf{R}_{02} + \mathbf{R}_{12}^{-1}\mathbf{H}_{12}\mathbf{R}_{12}. \tag{3}$$

The diatomic Hamiltonians are constructed as a block matrices, for example,

$$\mathbf{H}_{01} = \begin{bmatrix} \tilde{Q}_{01} & \tilde{J}_{01} & 0_6 \\ \tilde{J}_{01} & \tilde{Q}_{01} & 0_6 \\ 0_6 & 0_6 & 0_6 \end{bmatrix} + \begin{bmatrix} V_{\mathrm{neu}}(r_{12}) \otimes I_6 & 0_6 & 0_6 \\ 0_6 & V_{\mathrm{neu}}(r_{12}) \otimes I_6 & 0_6 \\ 0_6 & 0_6 & 0_6 \end{bmatrix}, \tag{4}$$

with V_{neu} as neutral Xe_2 ground state potential and $\tilde{Q}_{ij}$ and $\tilde{J}_{ij}$ as the Coulombic and exchange matrices, respectively,

TABLE I. Xe_2^+ fitted potential parameters for Eqs. (8) and (9) to MRCI calculated values with an aug-cc-pV5Z-PP basis.

	A (eV)	B (eV)	α (Å^{-1})	β (Å^{-1})	r_0 (Å)	n
Q_Σ	23111	20 565	2.159 7	2.131 8	0	1
Q_Π	174.6424	4.959 63	2.992 71	0.828 35	1.251 73	2
J_Σ	−5902.6927	5 902.911 7	0.944 92	0.943 22	N/A	N/A
J_Π	87.8381	0	1.742 1	0	N/A	N/A

$$\tilde{Q}_{ij} = \begin{bmatrix} Q_\Pi(r_{ij}) & 0 & 0 & 0 & 0 & 0 \\ 0 & Q_\Pi(r_{ij}) & 0 & 0 & 0 & 0 \\ 0 & 0 & Q_\Sigma(r_{ij}) & 0 & 0 & 0 \\ 0 & 0 & 0 & Q_\Pi(r_{ij}) & 0 & 0 \\ 0 & 0 & 0 & 0 & Q_\Pi(r_{ij}) & 0 \\ 0 & 0 & 0 & 0 & 0 & Q_\Sigma(r_{ij}) \end{bmatrix}, \tag{5}$$

$$\tilde{J}_{ij} = \begin{bmatrix} J_\Pi(r_{ij}) & 0 & 0 & 0 & 0 & 0 \\ 0 & J_\Pi(r_{ij}) & 0 & 0 & 0 & 0 \\ 0 & 0 & J_\Sigma(r_{ij}) & 0 & 0 & 0 \\ 0 & 0 & 0 & J_\Pi(r_{ij}) & 0 & 0 \\ 0 & 0 & 0 & 0 & J_\Pi(r_{ij}) & 0 \\ 0 & 0 & 0 & 0 & 0 & J_\Sigma(r_{ij}) \end{bmatrix}. \tag{6}$$

Specifics of the parametrization of the Xe_2^+ Coulombic Q and exchange potentials J are included below, and further details of the methodology and construction of $\mathbf{H}_{S.O.}$ are provided in Ref. 14. The rotational matrices $\mathbf{R}_{ij}$ were constructed by first expanding the 3×3 dimensional direction cosine matrices $\tilde{R}'_{ij}(\phi,\theta)$ to account for Kramers' pairs,

$$\tilde{R}'_{ij}(\phi,\theta) = \tilde{R}_{ij}(\phi,\theta) \oplus \tilde{R}_{ij}(\phi,\theta), \tag{7}$$

with ϕ and θ as the Euler angles required to rotate $\mathbf{H}_{ij}$ from the molecular to the laboratory frame.[25] The final rotational matrix $\mathbf{R}_{ij}$ then consisted of $\tilde{R}'_{ij}(\phi,\theta)$ set in the ii and jj blocks and null matrices filling the remaining blocks.

For a molecule in a given configuration, the energetics $\{E_{el,i}\}$ and wavefuctions $\{\phi_i\}$ of the 18 valence states were, respectively, defined as the eigenvalues and eigenvectors obtained by diagonalizing $\mathbf{H}$. The transition dipoles between the ground and excited states were calculated by the point charge method.[26]

To generate the input for the DIM calculations, *ab initio* pair potentials for the four Xe_2^+ valance states Σ_u, Π_g, Π_u, and Σ_g were obtained by the coupled clusters method, with single doubles and perturbative triple excitations (CCSD(T)). Similarly, these potentials were calculated by using multireference configuration interaction (MRCI) calculations and compared in Fig. 1(a). All *ab initio* calculations were carried out with the MOLPRO 2002.6 software package.[27] The Xe basis set used consisted of the augmented correlation consistent polarized valence X-zeta with a small core ($1s$-$3d$) relativistic pseudopotential, aug-cc-pV5Z-PP, basis set developed by Peterson *et al.*[28] A counterpoise correction was applied to the CCSD(T) potentials with a typical correctional value of 11.9 meV for the Σ_u potential at an internuclear separation distance of 3.1 Å, and a maximum correction of 23.1 meV for the Π_u potential at an internuclear separation distance of 2.4 Å. In both CCSD(T) and MRCI calculations, the Xe atomic $4s$, $4p$, and $4d$ orbitals were closed, and the active space consisted of the $5s$ and $5p$ valence orbitals. The asymptotic limit for the MRCI calculation was taken at 100 Å. The T_1 diagnostic for the CCSD(T) calculation never exceeded 0.012, which is less than the cited limit of 0.02 for CCSD theory.[29]

By defining the Xe_2^+ valance state pair potentials calculated above as, $V_{\Sigma_u}(r)$, $V_{\Pi_g}(r)$, $V_{\Pi_u}(r)$, and $V_{\Sigma_g}(r)$, the Coulombic and exchange potentials in Eqs. (5) and (6) can be decomposed as, $Q_{\Sigma/\Pi}(r)=\frac{1}{2}(V_{\Sigma/\Pi_u}(r)+V_{\Sigma/\Pi_g}(r))$ and $J_{\Sigma/\Pi}(r)=\frac{1}{2}(V_{\Sigma/\Pi_u}(r)-V_{\Sigma/\Pi_g}(r))$, respectively.[21]

The Coulombic pair potentials were fitted to the following form:

$$Q_{\Sigma/\Pi}(r) = Ae^{-\alpha(r-r_0)} - Be^{-\beta(r-r_0)^n} - \frac{c_4}{r^4}, \tag{8}$$

with the induction term $c_4=29.1$ eV/Å (Ref. 4) and exponential parameters given in Table I. The exchange potentials fit well to an exponential decay form,

$$J_{\Sigma/\Pi}(r) = Ae^{-\alpha r} - Be^{-\beta r}. \tag{9}$$

We chose to fit the MRCI potentials due to the greater dispersion [Fig. 1(b)] present in the attractive tail in the MRCI

Coulombic potentials and the negligible contribution of the counterpoise correction in the CCSD(T) calculations. This enhanced binding was attributed to a small degree of multireference character in that region. The neutral diatomic Xe potential V_{neu} was taken from Slavicek *et al.*[30]

B. Nonadiabatic coupling algebraic formalism

As rather thorough reviews of semiempirical nonadiabatic dynamical methods have been written by Coker[1] and Tully,[3,31] the following brief discussion will be constrained to the algebraic formalism with relevance to this study. For both the mean-field and surface-hopping methods, the electronic wavefuction was represented as a superposition of the adiabatic eigenstates ($n=18$), $\Phi_1,\Phi_2,\ldots,\Phi_n$,

$$\Psi_{\mathrm{el}}(t)=\sum_{j=1}^{n} a_j(t)e^{-(i/\hbar)\int_0^t E_j(\tau)d\tau}\Phi_j(R(t)), \tag{10}$$

with conservation of the norm of the expansion coefficients, i.e., $\Sigma_{j=1}^{n}|a_j(t)|^2=1$, and $R(t)$ as the set of nuclear positions. The expansion coefficients are propagated by insertion of Eq. (10) into the time dependent Schrödinger equation,

$$\frac{d\Psi}{dt}=-\frac{i}{\hbar}\mathbf{H}\Psi, \tag{11}$$

yielding,

$$\frac{da_j(t)}{dt}=-\sum_{k=1,k\neq j}^{n} a_k(t)d_{jk}e^{-(i/\hbar)\int_0^t E_k(\tau)-E_j(\tau)d\tau}, \tag{12}$$

with k iterating over a total of 18 states and d_{jk} as the nonadiabatic coupling terms that can be analytically expressed,

$$d_{jk}=\left\langle \Phi_j\middle|\frac{d\Phi_k}{dt}\right\rangle=\sum_{m=1}^{3N}\frac{\left\langle \Phi_j\middle|\frac{d\mathbf{H}}{dq_m}\middle|\Phi_k\right\rangle}{E_k-E_j}\cdot\frac{dq_m}{dt}, \tag{13}$$

as a summation over the $3N$ nuclear degrees of freedom q, i.e., atomic Cartesian coordinates. To integrate the coefficients in Eq. (12), we used the Crank–Nicolson method[32] with time-step sizes indicated in the text. MD was implemented with the velocity Verlet algorithm[33] and energy conservation was monitored.

A technical problem present for calculating the nonadiabatic coupling terms, d_{jk} in Eq. (12), arises upon the addition of spin-orbit coupling, which necessitates the use of complex wavefunctions. The origin of the difficulty is that the phases of the eigenfunctions are not uniquely provided by diagonalization of the Hamiltonian and are not necessarily consistent from one iteration to the next. Various approaches have been proposed to address this issue, and a method similar to that introduced by Krylov *et al.*[8] was used in this study. To provide phase consistency from one iteration to the next, the set (pair) of degenerate eigenfunctions of random phase $\{\phi_i\}$ were compared against a previously determined set of reference eigenfunctions $\{\Phi_i\}$, and the random phases were adjusted through a unitary transform U to provide the best match for a "phase defined" eigenfunction set $\{\varphi_i\}$, i.e.,

$$\varphi=\phi U. \tag{14}$$

To calculate U, the overlap term S_ϕ was defined as $S_\phi=\Phi^+\phi$. A singular value decomposition of S_ϕ yielded $S_\phi=u\sigma v^+$, where σ is diagonal matrix with positive real elements. U was then obtained as $U=vu^+$.

Although it can be easily shown that the nonadiabatic coupling terms within a state, i.e., d_{jj} are zero for the case of real eigenfuctions, this is not necessarily true for complex eigenfuctions. Additionally, with the application of spin-orbit coupling, nonadiabatic coupling may exist between the Kramers' pairs. For both these cases, Eq. (13) cannot be directly applied; see Ref. 8 for discussion and proposed algorithmic solution. In this study, these terms were set to zero as has been done in previous studies.[16,34]

For the mean-field approach where the potential energy is expressed as

$$E=\langle\Psi|\mathbf{H}|\Psi\rangle=\sum_{i=1}^{n}|a_i|^2E_i, \tag{15}$$

and the forces for the q_m degree of freedom can be derived to be (see Appendix)

$$\begin{aligned}F_{q_m}&=-\frac{dE}{dq_m}\\&=-\sum_{\text{state }i}a_i^*a_i\left\langle\Phi_i\middle|\frac{dH}{dq_m}\middle|\Phi_i\right\rangle\\&\quad+\frac{E_i}{v_m}\left(\frac{da_i^*(t)}{dt}a_i(t)+a_i^*(t)\frac{da_i(t)}{dt}\right).\end{aligned} \tag{16}$$

Note that this differs from the Hellmann–Feynman theorem by the presence of the second term on the right. The theorem is dependent though on the condition that Ψ is an eigenstate of the Hamiltonian. The value second term was found to be small and it was not included for forces calculated by the mean-field method in this study.

Since the spin-orbit coupling constant was taken in this study to be independent of molecular configuration, only the gradient of the electronic Hamiltonian $\mathbf{H}_{\mathrm{el}}$ was required for force calculations Eq. (16). The Hamiltonian gradients were determined by differentiating Eq. (3). To illustrate, assuming the mode of interest is along the x-coordinate of atom 0,

$$\frac{d\mathbf{H}_{\mathrm{el}}}{dx_0}=\frac{d}{dx_0}[\mathbf{R}_{01}^{-1}\mathbf{H}_{01}\mathbf{R}_{01}+\mathbf{R}_{02}^{-1}\mathbf{H}_{02}\mathbf{R}_{02}+\mathbf{R}_{12}^{-1}\mathbf{H}_{12}\mathbf{R}_{12}]. \tag{17}$$

Differentiating the first term yields

$$\begin{aligned}&\frac{d}{dx_0}[\mathbf{R}_{01}^{-1}\mathbf{H}_{01}\mathbf{R}_{01}]\\&=\frac{d\mathbf{R}_{01}^{-1}}{dx_0}\mathbf{H}_{01}\mathbf{R}_{01}+\mathbf{R}_{01}^{-1}\frac{d\mathbf{H}_{01}}{dx_0}\mathbf{R}_{01}+\mathbf{R}_{01}^{-1}\mathbf{H}_{01}\frac{d\mathbf{R}_{01}}{dx_0}.\end{aligned} \tag{18}$$

Application of the chain rule to the block rotational matrices yields

TABLE II. Assorted Xe_3^+ electronic ground state constants.

	This study	Literature values
r_e (Å)	3.322	3.263,[a] 3.270–3.47[b]
ω_e^{sym} (cm^{-1})	32.9	73.2[a]
ω_e^{bnd} (cm^{-1})	20.3	
ω_e^{asy} (cm^{-1})	67.3	72.6[a]
$Xe_3^+ \rightarrow Xe_2^+ + Xe$ Dissociation energy (eV)	0.222	0.197–0.36[a,b]

[a]Reference 37.
[b]Reference 39 and references within.

$$\frac{d\mathbf{R}_{01}}{dx_0} = \frac{d\mathbf{R}_{01}}{d\phi} \cdot \frac{d\phi}{dx} + \frac{d\mathbf{R}_{01}}{d\theta} \cdot \frac{d\theta}{dx}, \tag{19}$$

with Euler angles ϕ and θ. In this manner, all gradient quantities were analytically determined.

The surface-hopping method evolves the nuclear dynamics on a single potential energy surface (PES) with an evaluation of the probability of "hopping" surfaces determined at every time step. The hopping probability is compared against a randomly generated number between 0 and 1, and the hop is considered successful if the hopping probability exceeds the random value. Following the Tully's fewest switches approach,[5] the hopping probability can be derived as

$$P_{j\rightarrow k} = \frac{2\Delta t \, \mathrm{Re}(a_j^*(t)a_k(t)d_{jk}(t)e^{-(i/\hbar)\int_0^t E_k(\tau)-E_j(\tau)d\tau})}{a_j^*(t)a_j(t)}. \tag{20}$$

As the system abruptly changes PESs upon successful hops, the kinetic energy of the system must be adjusted to maintain energy conservation. We have chosen the method[35] in which the momenta of the nuclei are rescaled along the vector of the gradient of the difference of the initial and final PESs $\vec{\nabla}(E_i - E_f)$.

III. RESULTS AND DISCUSSION

A. Characterization of the ground state, $\Sigma(1/2)_u$

To gain an understanding of the initial state for the dynamics of Xe_3^+, the ground state nuclear wavefunction was constructed from its four vibrational modes $(3N-5)$. In the convention of normal mode coordinates,[36] the effective mass along each mode is equal to the mass m of atomic Xe. The symmetric, asymmetric, and bending mode force constant values were determined by finite difference along the mode coordinates. The corresponding frequencies,

$$\omega_e = \frac{1}{2\pi}\sqrt{\frac{k}{m}}, \tag{21}$$

are tabulated in Table II. Comparison of frequencies calculated in the above manner with the *ab initio* calculation reported by Seidel *et al.*[37] shows slight differences in the asymmetric stretch frequency, 67.3 vs 72.6 cm^{-1}, respectively, and more pronounced differences, in the symmetric stretch frequencies: 32.9 vs 73.2 cm^{-1}. We also note that the equilibrium bond length calculated in this study, 3.32 Å, is slightly longer than the 3.26 Å value obtained by Seidel *et al.*, and

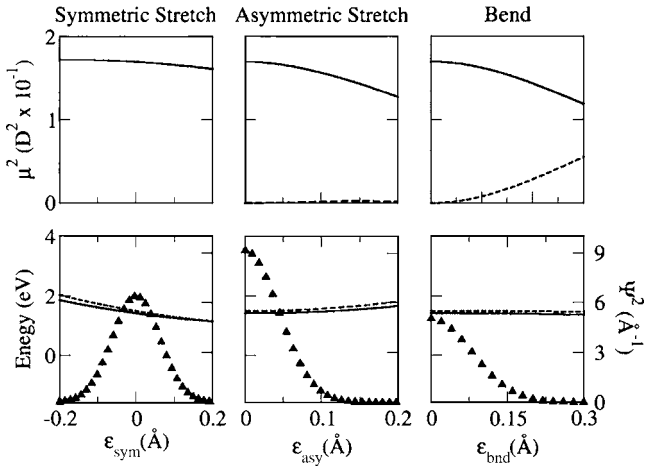

FIG. 2. Bottom: Xe_3^+ $\Pi(1/2)_g$ (solid line) and $\Pi(1/2)_u$ (dashed line) PESs for the symmetric, asymmetric, and bending modes centered about the equilibrium geometry. The respective ground states $\psi^2(\varepsilon)$ for each mode are superimposed (triangle) with magnitudes corresponding to the right axis. Top: Squared transition dipole values for $\Sigma(1/2)_u \rightarrow \Pi(1/2)_g$ and $\Sigma(1/2)_u \rightarrow \Pi(1/2)_u$ represented as solid and dashed lines, respectively.

the 3.26–3.27 Å values obtained in recent DIM studies.[38,39] The binding energy of the $Xe_3^+ \rightarrow Xe_2^+ + Xe$ dissociation was calculated by constraining the distance of two nearest neighbor atoms and recording the lowest potential energy of the trimer with the third atom spanning positions of distance and angular separations from the fixed pair. The constraint was then increased in length and the procedure was repeated. In effect, this generated a potential of mean force for the triatomic at 0 K. In this manner, a binding value of 0.22 eV was obtained and compared to recent calculated values of 0.24–0.25 eV by Doltsinis[38] and 0.27–0.28 eV by Kalus and Hrivnak.[39]

The harmonic vibrational wavefunctions can be written as

$$\psi_{l,j}(\varepsilon) = N_j H_j(y) e^{-y^2/2}, \tag{22}$$

for mode l, vibrational state j, atomic Xe mass m, Hermite polynomial H_j, and displacement ε(Å) along the Cartesian normal mode coordinates, where

$$y = \varepsilon\sqrt{\frac{m\omega_l}{\hbar}}, \tag{23}$$

and the normalization constant N_j as

$$N_j = \left(\frac{m\omega_l}{\pi\hbar}\right)^{1/4} \frac{1}{\sqrt{2^j j!}}. \tag{24}$$

The squared wavefunctions are plotted in Fig. 2. Temperature dependence was incorporated by weighting excited vibrational states by the Boltzmann distribution and summing over the states, for example,

$$\psi_{sym}^2(\varepsilon_1, T) = \sum_{i=0}^{\infty} \psi_{sym}^2(i, \varepsilon_1)\frac{e^{-E_i/kT}}{q}, \tag{25}$$

for state i, Boltzmann constant k, temperature T, and q as the vibrational partition function. In the harmonic approximation used in this study,

$$q = \frac{1}{1 - e^{-2E_0/kT}}, \tag{26}$$

where E_0 is the corresponding zero point energy of the mode. The total analytical wavefunction can be written as a product of its four constituent modes,

$$\Psi_{\text{nucl}}(\varepsilon_1, \varepsilon_2, \varepsilon_3, \varepsilon_4) = \psi_{\text{sym}}(\varepsilon_1)\psi_{\text{bnd }A}(\varepsilon_2)\psi_{\text{bnd }B}(\varepsilon_3)\psi_{\text{asy}}(\varepsilon_4), \tag{27}$$

with displacements ε_1, ε_2, ε_3, and ε_4 from the ground state potential energy minimum.

B. Photoexcitation dynamics

To validate the treatment used in this study to construct the Xe_3^+ PES and simulate nonadiabatic dynamics, a quantitative comparison can be made to the experimental kinetic energy distribution[40] of the photofragments as a function of excitation energy.[19,41] The initial configuration of the Xe_3^+ molecule was represented as a series of 22 grid points per mode spanning the analytical ground state wavefunction. By symmetry, the bending and asymmetric stretching modes could be reduced to 11 grid points each, thus resulting in a calculation consisting of $22 \times 11 \times 11 \times 11$ or 29 282 total trajectories for the mean-field approach. The surface-hopping calculations in this study employed 100 trajectories for each initial configuration, thus requiring calculation of over 2.9×10^6 trajectories.

Since zero point energy values for each mode were $\sim 1/1000$ of the energy difference between electronic states, their values were neglected in calculation of the excitation energy. The excitation was simulated by the reflection method,[42] and the mean-field approach was used to treat the subsequent dynamics. Since all excited states contained little to no binding, the molecule dissociated and the calculation was terminated when all atoms were separated by a distance greater than 6 Å. The resultant kinetic energy values of dissociated atoms were then weighted by the their initial absorption cross section and binned.

The experimental and resultant simulated kinetic energy distributions are shown in Fig. 3. The kinetic energy distributions were calculated by the mean-field approach with a 0.1 fs step size and a grid of 11 points per normal mode. By decomposing the spectrum to display the initial excitation state of the photofragment (Fig. 3), it was apparent that the excess kinetic energy (KE) closely fell along the predicted dissociated energy limits of the $^2P_{3/2}$ (solid line) and $^2P_{1/2}$ states (dashed line),

$$\text{KE}(^2P_{3/2}) = h\nu - D_e, \tag{28}$$

$$\text{KE}(^2P_{1/2}) = h\nu - D_e - \Delta, \tag{29}$$

with excitation energy $h\nu$, binding energy D_e, and Xe^+ spin-orbit splitting Δ. See Fig. 1(c) for a description of parameter notation. In agreement with Hrivnak *et al.*,[41] no transfer of population was observed between the $^2P_{1/2}$ states: $\Pi(1/2)_g$, $\Pi(1/2)_u$, $\Sigma(1/2)_u$, and the less energetic $^2P_{3/2}$ valance states. The temperature dependence of the KE spectrum was investigated up to 75 K, with no noticeable difference in spectral values. A set of identical simulations without incorporation of nonadiabatic dynamics, i.e., adiabatic dynamics, also generated very similar spectral values at 0–75 K (not shown).

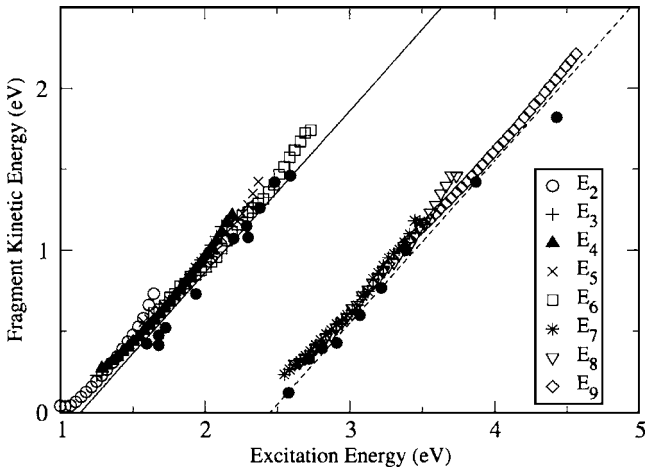

FIG. 3. Kinetic energy of dissociated Xe_3^+ photofragments as a function of excitation energy, partitioned by excited electronic state contribution. Experimental points (●) are from Ref. 19. Solid and dotted lines, respectively, denote the theoretical $^2P_{3/2}$ and $^2P_{1/2}$ fragment kinetic energies (see discussion in text). For clarity in notation, Kramers' pair states are represented as a single electronic state, i.e., excited electronic states are labeled E_2–E_9.

A measure of the nonadiabatic coupling between the $\Pi(1/2)_g$ and $\Pi(1/2)_u$ states was reflected in the experimental symmetric fragmentation spectrum of Haberland *et al.*[19] Excitation of the Xe_3^+ in the range of 1.5–4.5 eV generated neutral and charged Xe monatomic species. In accordance to previous studies,[19,41] no dimers were generated by the photodissociation process in this energy range. The distribution of molecules dissociated via the asymmetrically charged Π_g and symmetrically charged Π_u states was then determined based on the intensity of the slow and fast peaks of the charged and neutral fragments in time-of-flight spectra. The degree of symmetric fragmentation is thus representative of the resultant population of a Xe_3^+ in the $\Pi(1/2)_u$ state, within the reported excitation energy window. Our approach to simulate this spectrum is outlined as follows:

(1) Before electronic excitation, the system was localized about the minimum of the ground $\Sigma(1/2)_u$ state with a given amount of zero point energy in each vibrational mode. The initial configuration specified was specified as $\{\varepsilon_{\text{sym}}, \varepsilon_{\text{bndA}}, \varepsilon_{\text{bndB}}, \varepsilon_{\text{asy}}\}$.
(2) Electronic excitation transferred population of the configuration to an accessible excited state, i.e., $\Sigma(1/2)_u \rightarrow \Pi(1/2)_g$ or $\Pi(1/2)_u$.
(3) Nuclear dynamics began on this excited adiabatic state.
(4) The system approached the crossing point [see circled region, Fig. 1(c)] of $\Pi(1/2)_g$ and $\Pi(1/2)_u$, and nonadiabatic transitions take place.
(5) After complete dissociation, the population of the lower $\Pi(1/2)_u$ state was evaluated as the square of the nonadiabatic expansion coefficient in $|a_{\Pi(1/2)_u}|^2$ for calculations based on the mean-field approach or as the fraction of 100 trajectories ending in that state for the surface-hopping calculations.
(6) After completion of the MD simulations, each trajec-

TABLE III. Energy conservation deviation (meV).

Method	Time step (fs)	Average	Std. deviation	Maximum
Mean-field	1	10	10.6	584
Mean-field	5	17	26	1025
Surface-hopping	5	4.5	3.4	96

tory was then binned according to its initial excitation energy. Its probability was given a statistical weight based on the square of the nuclear wavefunction, $\Psi^2_{\text{nucl}}(\varepsilon_1,\varepsilon_2,\varepsilon_3,\varepsilon_4)$ of the initial configuration and square of the transition dipole $|\mu_{1j}|^2$ from the ground, state 1, to the jth state accessed in the excitation of step 2. The probability weights for each configuration were then normalized to the total weight of all configurations in the bin.

Due to the large number of trajectories required, aggressive time steps were needed to reduce computational expense. This allowed some trajectories to possess larger deviations in energy conservation, although the average and standard deviations remained low (Table III). Subsequent calculations with smaller time steps ensured that the energy conservation properly scaled with the inverse of step size.[33]

A comparison of the spectrum calculated by each approach is shown in Fig. 4. First, the mean-field approach appears to closely agree with the more computationally demanding surface-hopping approach. This was not surprising, since both the $\Pi(1/2)_u$ and $\Pi(1/2)_g$ states converge to the same dissociated energy of the $^2P_{1/2}$ state [Fig. 1(c)], and differences have been noted between application of the two approaches when states diverge.[3] By overlaying the experimental spectral values[19] (Fig. 4), we observe that the simulated spectra at all temperatures are generally centered about apex of the experimental spectrum, and the apex value falls within the simulated spectral range of temperatures at that excitation energy, approximately 3.1, specifically matched by the 25 K spectra. Convergence of the spectrum was checked with respect to resolution (11 vs 22 points per mode), width (extending the 11 point grid to include 11 additional points well into the mode wavefuntion tails) of the grid, and the time-step size.

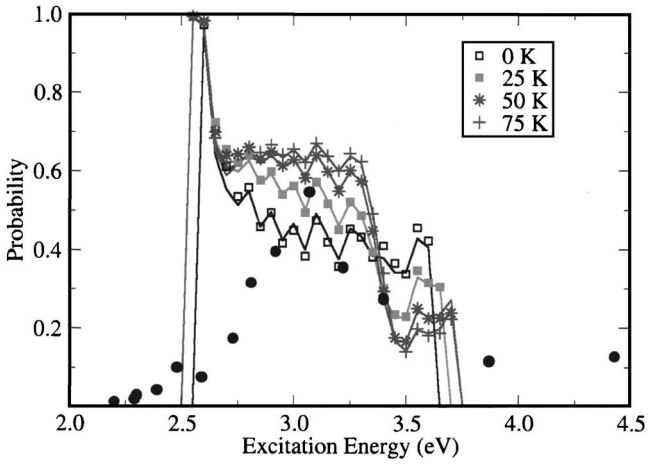

FIG. 4. Probability of molecular Xe_3^+ dissociation to the lowest $^2P_{1/2}$ state as a function of excitation energy. For symmetric configurations, cf. Fig. 1(c), the lowest state corresponds to $\Pi(1/2)_u$. Results from simulations: Mean-field (solid lines), and surface-hopping (0 K: □, 25 K: ■, 50 K: *, 75 K: +) are superimposed on the experimental values of the symmetric fragmentation spectrum (●), obtained by Haberland *et al.* (Ref. 19).

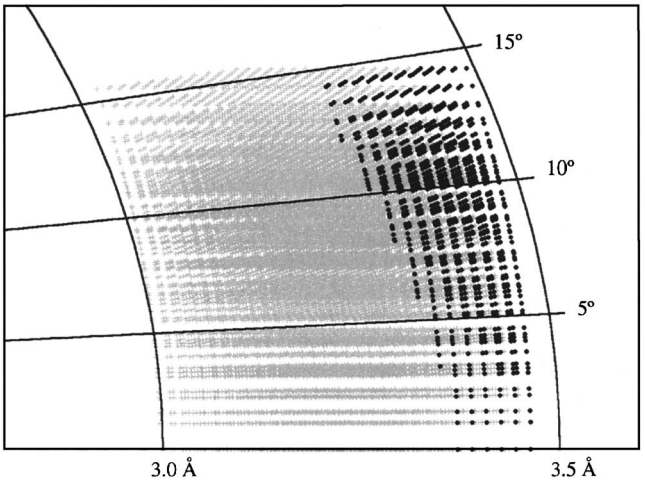

FIG. 5. Polar coordinate plot of initial coordinates sampled (+) based on the ground state probability distribution $\Psi^2_{\text{nucl}}(\varepsilon_1,\varepsilon_2,\varepsilon_3,\varepsilon_4)$. Trajectories that contribute to the "red peak" (see Fig. 5) with excitation energies <2.7 eV and that possess a probability of greater than 0.95 are highlighted (●).

A notable difference between the experimental and simulated spectra is the red peak at 2.6 eV. This peak is present at all temperatures and using both the mean-field and surface-hopping approaches. Insight to the origin of the peak can be obtained by inspection of the initial coordinates from which resultant trajectories contribute. By orienting two atoms of the Xe_3^+ molecule along a fixed axis, the position of the third can display the angular range of initial coordinates sampled. A plot in polar coordinates (Fig. 5) displays the initial coordinates that contribute to the red peak with a probability greater than 0.95, superimposed on the all positions sampled. It is apparent that trajectories from highly bent and stretched coordinates contribute most greatly. An example of one such trajectory, shown in Fig. 6, reveals that unlike the linear case, the $\Pi(1/2)_g$ and $\Pi(1/2)_u$ PESs do not cross. This resulted in the population, almost perfectly following the initial, lower, state. In a sense, similar trajectories overemphasized the nonadiabatic crossing behavior. The most likely source for this deviation can be attributed to possible inaccuracies in the PES. This may also be reflected by discrepancies in the calculated frequencies of the $\Sigma(1/2)_u$ ground state from *ab initio* values, in particular ω_e^{sym} by a factor of over 2 (Table II). Second, the $Xe_3^+ \rightarrow Xe_2^+ + Xe$ dissociation energy is 10%–20% lower in comparison to calculated values reported recently.[37–39] Two approximations made in this study, the neglect of overlap of the atomic wavefunctions upon which the basis states in Eq. (1), are constructed,[43] and the neglect of induced-dipole, induced-dipole interactions in the molecular Hamiltonian,[38,39] Eq. (2), may limit the accuracy of the PES. Small inaccuracies in the ground PES would have a large influence on the ground state nuclear vibrational wavefunctions, which in turn would affect the initial coordinates calculated to be sampled. While it is beyond the scope of this paper, one could conceive of an approach to "tune" various

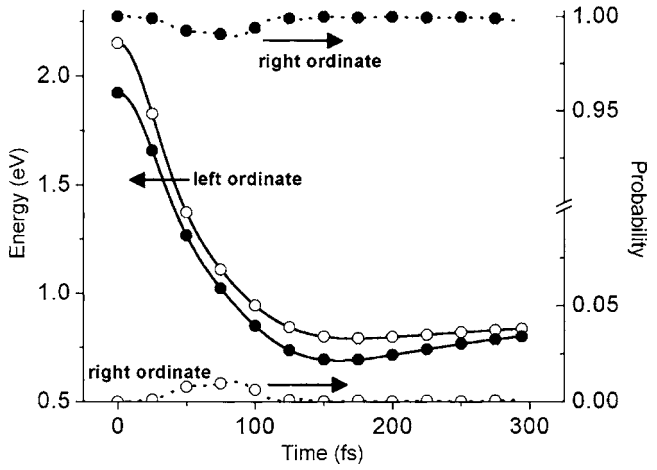

FIG. 6. Representative trajectory from a bent initial configuration contributing to red peak in Fig. 5 with ε_{sym}, ε_{bndA}, ε_{bndB}, ε_{asy} as −0.2, 0.25, 0.25, and 0.15 Å, respectively. The potential energies of electronic states $\Pi(1/2)_g$ (solid line, solid circle) and $\Pi(1/2)_u$ (solid line, hollow circle) are shown to not cross over the evolution of the trajectory. Thus no significant adiabatic transfer of population occurs between the $\Pi(1/2)_g$ and $\Pi(1/2)_u$ states (dotted line and solid and hollow circles, respectively, right ordinate).

PES parameters and temperature values to match the experimental spectrum in Fig. 5.

As discussed above, the Xe_3^+ ground state vibrational wavefunction consisted of a product of its constituent modes in Eq. (22) and the spectrum contains nonadiabatic contributions from all mode combinations spanned by Ψ^2_{nucl}. Nevertheless, it could be insightful to consider the contributions of solely individual modes by themselves. The calculated $\Pi(1/2)_g \rightarrow \Pi(1/2)_u$ crossing probabilities along the bending and asymmetric stretching modes are shown in Fig. 7. This was accomplished by spanning the deviation parameter ε_i for the mode of interest while restricting the deviation parameters for the remaining modes to zero. Note that no transitions occur along the symmetrical coordinate due to symmetry. Both mean-field and surface-hopping approaches were employed with a 0.1 fs time step. The surface-hopping calculations consisted of 200 trajectories at each step. It is apparent that bending mode nonadiabatically couples the two states to a much greater extent than the asymmetric stretching mode (Fig. 7). This point is reinforced when one considers that the bending ground state wavefunction is broader than the asymmetric stretch, and thus possesses greater population at larger displacement values. This difference in transition probabilities was not parsed out of analysis of the original measurements.[19]

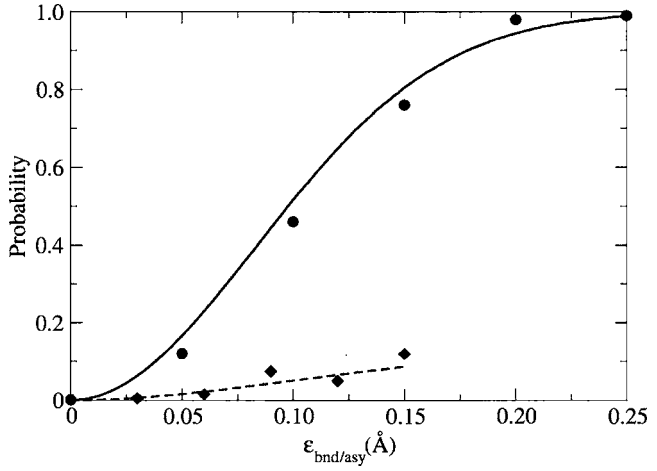

FIG. 7. $\Pi(1/2)_g \rightarrow \Pi(1/2)_u$ nonadiabatic crossing probability along the bending and asymmetric stretch modes. The solid line and filled circles correspond to mean-field and surface-hopping calculations, respectively, along the bending mode. The dotted line and diamond symbols correspond to the surface-hopping and mean-field calculated values along the asymmetric stretching mode.

IV. CONCLUSION

This theoretical study explored both (A) the adequacy of the mean-field and surface-hopping approaches for modeling nonadiabatic transitions in the photodissociation of a simple molecular system, Xe_3^+, containing a non-negligible degree of spin-orbit coupling, and (B) the nonadiabatic crossing probability between two states of interest $\Pi(1/2)_g \rightarrow \Pi(1/2)_u$ as a function the vibrational modes of the ground state. The analytical ground state vibrational wavefunction was constructed by calculation of the fundamental vibrational frequencies of the ground state potential energy surface. A grid of 11–22 coordinates along each normal mode was used for the representation of the ground electronic state wavefunction. Temperature dependence was considered and implemented by representation of the ground state electonic wavefunction with a superposition of excited vibrational states. The calculated spectrum of the kinetic energies of the atomic photofragments was found to match well to the experimental values. The $\Pi(1/2)_g \rightarrow \Pi(1/2)_u$ nonadiabatic crossing was studied by simulations of excitation of the ground electronic state to the $\Pi(1/2)_g$ and $\Pi(1/2)_u$ states and analysis of the final state upon dissociation. The simulated symmetric fragmentation spectrum was then compared to the experimental spectrum and found to possess a similar form and qualitative match in width and position. Quantitative deviations were discussed and attributed to the inaccuracies in the potential energy surface. Finally, it was determined that the bending mode coupled the nonadiabatic crossing between the $\Pi(1/2)_g$ and $\Pi(1/2)_u$ states to a much greater degree that found along the asymmetric stretch coordinate.

APPENDIX: DERIVATION OF ATOMIC FORCES BY THE MEAN-FIELD APPROACH

Derivation for the mean-field force acting on the q_m degree of freedom, Eq. (16) is given as follows. Substituting the electronic wavefunction from Eq. (A1),

$$\Psi(t) = a_0(t)e^{-i/\hbar\int_0^t E_0(\tau)d\tau}\Phi_0 + a_1(t)e^{-i/\hbar\int_0^t E_1(\tau)d\tau}\Phi_1 + \cdots \tag{A1}$$

into the time independent Schrödinger equation, allows solution for the electronic energy of a molecular system in a given configuration to be written as

$$E = \langle \Psi | H | \Psi \rangle = \langle a_0 \Phi_0 | H | a_0 \Phi_0 \rangle + \langle a_1 \Phi_1 | H | a_1 \Phi_1 \rangle + \cdots . \tag{A2}$$

Taking the gradient of energy with respect to the q_m degree of freedom yields

$$\frac{dE}{dq_m} = \frac{dE_0}{dq_m} + \frac{dE_1}{dq_m} + \cdots = \frac{d}{dq_m}\langle a_0 \Phi_0 | H | a_0 \Phi_0 \rangle + \frac{d}{dq_m}\langle a_1 \Phi_1 | H | a_1 \Phi_1 \rangle + \cdots . \tag{A3}$$

For illustration, the first term dE_0/dq_m can be expanded,

$$\frac{dE_0}{dq_m} = \left\langle \frac{da_0}{dq_m}\Phi_0 | H | a_0 \Phi_0 \right\rangle + \left\langle a_0 \frac{d\Phi_0}{dq_m} | H | a_0 \Phi_0 \right\rangle + \left\langle a_0 \Phi_0 \left| \frac{dH}{dq_m} \right| a_0 \Phi_0 \right\rangle + \left\langle a_0 \Phi_0 | H | a_0 \frac{d\Phi_0}{dq_m} \right\rangle + \left\langle a_0 \Phi_0 | H | \frac{da_0}{dq_m}\Phi_0 \right\rangle . \tag{A4}$$

The expansion coefficient a_0 and corresponding spatial derivative da_0/dq_m can be removed from the integrals as they are not dependent on the electronic coordinate,

$$\frac{dE_0}{dq_m} = a_0^* a_0 \left\langle \Phi_0 \left| \frac{dH}{dq_m} \right| \Phi_0 \right\rangle + E_0 \left(\frac{da_0^*}{dq_m} a_0 + a_0^* \frac{da_0}{dq_m} \right) + a_0^* a_0 E_0 \left(\left\langle \frac{d\Phi_0}{dq_m} | \Phi_0 \right\rangle + \left\langle \Phi_0 | \frac{d\Phi_0}{dq_m} \right\rangle \right). \tag{A5}$$

The last term on the right of Eq. (A5) is zero,

$$\langle \Phi_0 | \Phi_0 \rangle = 1, \quad \frac{d}{dq_m}\langle \Phi_0 | \Phi_0 \rangle = 0, \quad \left\langle \frac{d\Phi_0}{dq_m} | \Phi_0 \right\rangle + \left\langle \Phi_0 | \frac{d\Phi_0}{dq_m} \right\rangle = 0 . \tag{A6}$$

From Eqs. (A3), (A5), and (A6), the total force on the degree of freedom q_m can thus be written as

$$F_{q_m} = -\frac{dE}{dq_m} = -\sum_{\text{state } i} a_i^* a_i \left\langle \Phi_i \left| \frac{dH}{dq_m} \right| \Phi_i \right\rangle + E_i \left(\frac{da_i^*}{dq_m} a_i + a_i^* \frac{da_i}{dq_m} \right). \tag{A7}$$

By application of the chain rule, spatial derivatives of the expansion coefficients in Eq. (A7) can be expressed in more familiar terms,

$$F_{q_m} = -\frac{dE}{dq_m} = -\sum_{\text{state } i} a_i^* a_i \left\langle \Phi_i \left| \frac{dH}{dq_m} \right| \Phi_i \right\rangle + \frac{E_i}{v_m} \left(\frac{da_i^*(t)}{dt} a_i(t) + a_i^*(t) \frac{da_i(t)}{dt} \right), \tag{A8}$$

with the reciprocal of the velocity v_m, substituted for the quotient, $v_m^{-1} = 1/dq_m/dt$. As stated in the text, the second term on the right differentiates Eq. (16) from the Hellmann–Feynman theorem. Reference 3 contains an extended discussion and derivation of this second term in an alternative form.

[1] D. F. Coker, in *Computer Simulations in Chemical Physics*, edited by M. P. Allen and D. J. Tildesley (Kluwer, Netherlands, 1993).
[2] N. L. Doltsinis and D. Marx, J. Theor. Comput. Chem. **1**, 319 (2002).
[3] J. C. Tully, in *Modern Methods for Multidimensional Dynamics Computations in Chemistry*, edited by D. L. Thompson (World Scientific, New Jersey, 1998).
[4] P. Ehrenfest, Z. Phys. **45**, 455 (1927).
[5] J. C. Tully, J. Chem. Phys. **93**, 1061 (1990).
[6] V. S. Batista and D. F. Coker, J. Chem. Phys. **106**, 6923 (1997).
[7] M. Ovchinnikov, B. L. Grigorenko, K. C. Janda, and V. A. Apkarian, J. Chem. Phys. **108**, 9351 (1998).
[8] A. I. Krylov, R. B. Gerber, and R. D. Coalson, J. Chem. Phys. **105**, 4626 (1996).
[9] G. D. Billing, C. Coletti, A. K. Kurnosov, and A. P. Napartovich, J. Phys. B **36**, 1175 (2003).
[10] J. R. Krenos, R. K. Preston, R. Wolfgang, and J. C. Tully, J. Chem. Phys. **60**, 1634 (1974).
[11] R. Mitric, V. Bonacic-Koutecky, J. Pittner, and H. Lischka, J. Chem. Phys. **125**, 024303 (2006).
[12] F. O. Ellison, J. Am. Chem. Soc. **85**, 3540 (1963).
[13] M. Amarouche, G. Durand, and J. P. Malrieu, J. Chem. Phys. **88**, 1010 (1988).
[14] S. L. Fiedler, K. Vaskonen, J. Ahokas, H. Kunttu, and V. A. Apkarian, J. Chem. Phys. **117**, 8867 (2002).
[15] L. Xiao and D. F. Coker, J. Chem. Phys. **100**, 8646 (1994).
[16] P. E. Maslen, J. M. Papanikolas, J. Fader, R. Parson, and S. V. ONeil, J. Chem. Phys. **101**, 5731 (1994).
[17] T. J. Martinez, Chem. Phys. Lett. **272**, 139 (1997).
[18] T. Ikegami, T. Kondow, and S. Iwata, J. Chem. Phys. **99**, 3588 (1993).
[19] H. Haberland, A. Hofmann, and B. v. Issendorff, J. Chem. Phys. **103**, 3450 (1995).
[20] S. L. Fiedler, J. Eloranta, K. Vaskonen, and H. Kunttu, J. Phys. Chem. A **109**, 4512 (2005).
[21] P. J. Kuntz and J. Valldorf, Z. Phys. D: At., Mol. Clusters **8**, 195 (1988).
[22] F. Mies, Phys. Rev. A **7**, 942 (1973).
[23] K. Yoshino and D. E. Freeman, J. Opt. Soc. Am. B **2**, 1268 (1985).
[24] P. Rupper, O. Zehnder, and F. Merkt, J. Chem. Phys. **121**, 8279 (2004).
[25] R. N. Zare, *Angular Momentum* (Wiley, New York, 1988).
[26] F. Y. Naumkin, Chem. Phys. **252**, 301 (2000).
[27] H.-J. Werner, P. J. Knowles, R. D. Amos, A. Bernhardsson, A. Berning, P. Celani, D. L. Cooper, M. J. O. Deegan, A. J. Dobbyn, F. Eckert, C. Hampel, G. Hetzer, P. J. Knowles, T. Korona, R. Lindh, A. W. Lloyd, S. J. McNicholas, F. R. Manby, W. Meyer, M. E. Mura, A. Nicklass, P. Palmieri, R. Pitzer, G. Rauhut, M. Schütz, U. Schumann, H. Stoll, A. J. Stone, R. Tarroni, T. Thorsteinsson, and H.-J. Werner, MOLPRO, version 2002.6, a package of *ab initio* programs.
[28] K. A. Peterson, D. Figgen, E. Goll, H. Stoll, and M. Dolg, J. Chem. Phys. **119**, 11113 (2003).
[29] T. J. Lee and P. R. Taylor, Int. J. Quantum Chem. **S23**, 199 (1989).
[30] P. Slavicek, R. Kalus, P. Paska, I. Odvarkova, P. Hobza, and A. Malijevsky, J. Chem. Phys. **119**, 2102 (2003).
[31] J. C. Tully, in *Modern Theoretical Chemistry 2*; edited by W. H. Miller (Plenum, New York, 1976).
[32] W. H. Press, B. P. Flannery, S. A. Teukolsky, and W. T. Vetterling, *Numerical Recipies in C: The Art of Scientific Computing* (Cambridge University Press, New York, 2002).
[33] M. P. Allen and D. J. Tildesley, *Computer Simulation of Liquids* (Oxford University Press, London, 1997).
[34] D. Bonhommeau, A. Viel, and N. Halberstadt, J. Chem. Phys. **123**, 054316 (2005).
[35] N. C. Blais, D. G. Truhlar, and C. A. Mead, J. Chem. Phys. **89**, 6204 (1988).
[36] P. F. Bernath, *Spectra of Atoms and Molecules* (Oxford University Press,

New York, 1995).
[37] S. Seidel, K. Seppelt, C. van Wüllen, and X. Y. Sun, Angew. Chem., Int. Ed. **46**, 6717 (2007).
[38] N. L. Doltsinis, Mol. Phys. **97**, 847 (1999).
[39] R. Kalus and D. Hrivnak, Chem. Phys. **278**, 21 (2002).
[40] F. X. Gadea and J. Durup, Laser Chem. **11**, 95 (1991).
[41] D. Hrivnak, R. Kalus, and F. X. Gadea, Europhys. Lett. **71**, 42 (2005).
[42] E. J. Heller, J. Chem. Phys. **68**, 2066 (1978).
[43] J. C. Tully, in *Modern Theoretical Chemistry*, edited by G. A. Segal (Plenum, New York, 1977).